Bioconjugate Chemistry

Article

pubs.acs.org/bc

In Vivo Imaging of GLP-1R with a Targeted Bimodal PET/Fluorescence Imaging Agent

Christian Brand,[†] Dalya Abdel-Atti,[†] Yachao Zhang,[†] Sean Carlin,[†] Susan M. Clardy,[‡] Edmund J. Keliher,[‡] Wolfgang A. Weber,[§,∥] Jason S. Lewis,[†,∥,⊥] and Thomas Reiner*[,†,⊥]

[†]Radiochemistry and Imaging Sciences Service and [§]Molecular Imaging and Therapy Service, Department of Radiology, [∥]Molecular Pharmacology and Chemistry Program, and [⊥]Center for Molecular Imaging and Nanotechnology, Memorial Sloan Kettering Cancer Center, New York, New York 10065, United States

[‡]Center for Systems Biology, Massachusetts General Hospital, 185 Cambridge Street, Boston, Massachusetts 02114, United States

Supporting Information

ABSTRACT: Accurate visualization and quantification of β-cell mass is critical for the improved understanding, diagnosis, and treatment of both type 1 diabetes (T1D) and insulinoma. Here, we describe the synthesis of a bimodal imaging probe (PET/fluorescence) for imaging GLP-1R expression in the pancreas and in pancreatic islet cell tumors. The conjugation of a bimodal imaging tag containing a near-infrared fluorescent dye, and the copper chelator sarcophagine to the GLP-1R targeting peptide exendin-4 provided the basis for the bimodal imaging probe. Conjugation was performed via a novel sequential one-pot synthetic procedure including ^{64}Cu radiolabeling and copper-catalyzed click-conjugation. The bimodal imaging agent ^{64}Cu-E4-Fl was synthesized in good radiochemical yield and specific activity (RCY = 36%, specific activity: 141 μCi/μg, >98% radiochemical purity). The agent showed good performance in vivo and ex vivo, visualizing small xenografts (<2 mm) with PET and pancreatic β-cell mass by phosphor autoradiography. Using the fluorescent properties of the probe, we were able to detect individual pancreatic islets, confirming specific binding to GLP-1R and surpassing the sensitivity of the radioactive label. The use of bimodal PET/fluorescent imaging probes is promising for preoperative imaging and fluorescence-assisted analysis of patient tissues. We believe that our procedure could become relevant as a protocol for the development of bimodal imaging agents.

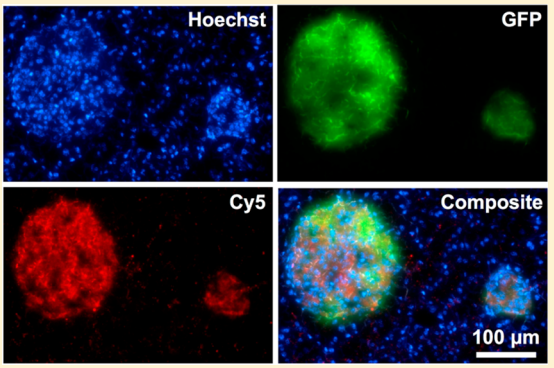

INTRODUCTION

Biomedical molecular imaging has evolved into a fast growing research field with the aims to characterize molecular processes at the cellular and subcellular level, using targeted vectors for in vivo imaging.[1−3] With the development of more specialized and sensitive technologies, novel avenues allow biomedical researchers to interrogate biological processes in vivo.[4] Two of the most generally used imaging technologies in biomedical research are positron emission tomography (PET) and optical fluorescence imaging. Both technologies have their own distinct characteristics, advantages, and limitations. PET imaging is a highly sensitive technology, which uses the γ-rays associated with positron annihilation events to localize positron emitting targeted tracers inside an organism. The low interaction of γ-rays in the human body allows physicians to accurately detect signals in patients even if they originate deep below the body surface. Based on physical limitations, however, PET systems only have spatial resolutions in the millimeter range.[5] Optical fluorescence imaging, on the other hand, has a much lower tissue penetration due to the strong absorption of visible and near-infrared (NIR) light in living tissues and can therefore not be used as a whole body imaging technology in humans. However, fluorescence images can be used to guide intraoperative procedures, and can provide subcellular resolution for ex vivo imaging or for in vivo window chamber imaging for preclinical research.[4,6] The combination of these modalities in a bimodal imaging probe overcomes the limitations of a single imaging technology and brings together high resolution, high sensitivity, and deep tissue penetration.

Over the past few years, different strategies have been applied to achieve multimodal capability of a molecular imaging agent.[2,7,8] Based on these previous approaches, we became interested in further exploring the scope, advantages, and performance of dual-labeled PET/optical imaging probes. Specifically, we aimed to design a dual-labeled agent for the glucagon-like peptide 1 receptor (GLP-1R) which is expressed on the membranes of β-cells in the pancreas as well as by insulinomas, tumors arising from pancreatic β-cells. The GLP-1R binding peptide exendin-4 has been used to image insulinomas and β-cells in animals as well as humans before,[9,10]

Received: April 21, 2014
Revised: May 20, 2014
Published: May 23, 2014

   dx.doi.org/10.1021/bc500178d | *Bioconjugate Chem.* 2014, 25, 1323−1330

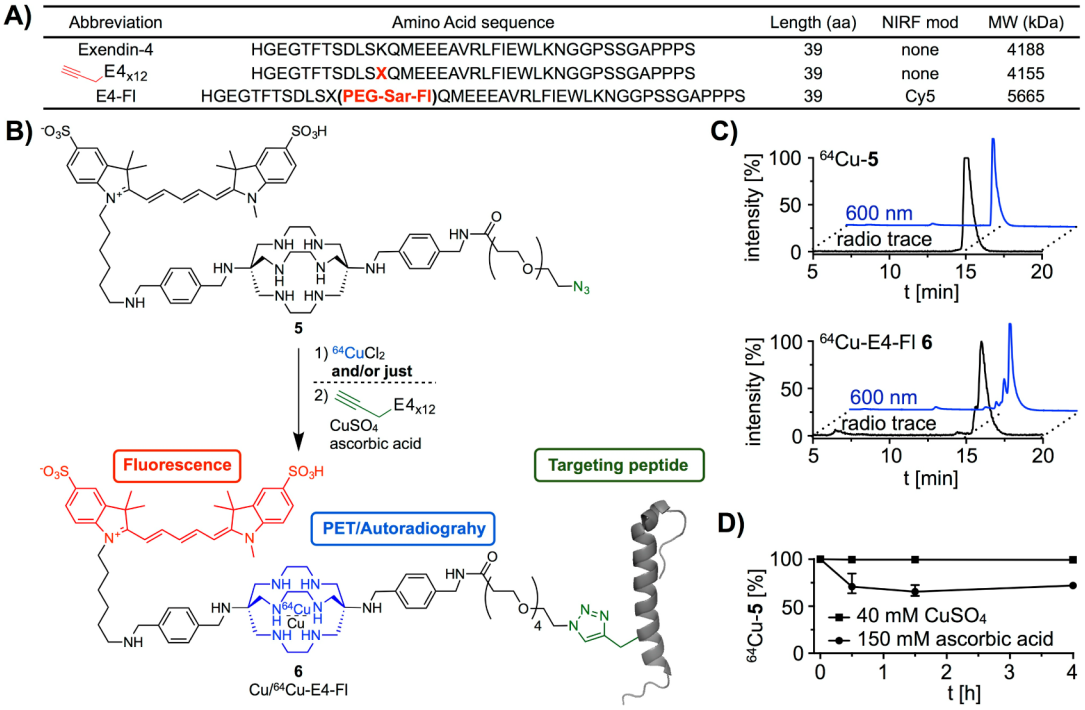

Figure 1. Amino acid sequence of targeting peptide, synthesis of imaging tracer Cu-E4-Fl **6** (cold peptide) as well as bimodal imaging tracer ^{64}Cu-E4-Fl **6** (radiolabeled peptide), and stability studies of ^{64}Cu-**5**. (A) Abbreviations and amino acid sequences of modified exendin-4 peptides. (B) Azide−alkyne Huisgen cycloaddition yielding imaging agent Cu-E4-Fl **6** and sequential one-pot synthesis (radiolabeling and copper-catalyzed azide−alkyne cycloaddition) of the bimodal imaging tracer ^{64}Cu-E4-Fl **6**. (C) HPLC chromatograms of ^{64}Cu-**5** and ^{64}Cu-E4-Fl **6**. (D) Competition and stability of ^{64}Cu-**5** in the presence of either $CuSO_4$ or ascorbic acid over 4 h.

as a fluorescent,[11,12] PET, or SPECT[13,14] imaging agent. Given the small size of the exendin-4 peptide, we aimed to synthesize a bimodal imaging tag for site-specific labeling at just one single site, which likely has a less negative impact on binding than conjugating different imaging modalities at different sites.

In order to characterize the dual-labeled exendin-4 probe ^{64}Cu-E4-Fl, we used 916−1 insulinoma xenografts as well as transgenic mice with islet-specific expression of enhanced green fluorescent protein (GFP). In these experiments we asked the following questions: (1) Is it possible to design a bimodal imaging agent based on exendin-4 with metabolic stability comparable to the monomodal labeled counterpart? (2) Is this bimodal imaging agent, ^{64}Cu-E4-Fl, binding to its target GLP-1R with high affinity? (3) Can both PET as well as optical imaging be performed on a mouse which has received an amount of imaging agent suitable for both modalities?

As a result of our findings, we showed that the ^{64}Cu-radiolabeled sarcophagine chelator is stable enough to allow for copper-catalyzed azide−alkyne cycloaddition. We synthesized the dual-modality imaging agent ^{64}Cu-E4-Fl via a one-pot protocol and confirmed binding to GLP-1R in insulinomas as well as pancreatic β-cell mass using PET and fluorescent imaging.

RESULTS

The four-step synthesis toward the sarcophagine-based and fluorescently labeled copper chelator **5** is shown in the Supporting Information (Scheme S1). In comparison to previous approaches to functionalize sarcophagine,[15,16] we achieved alkylation of DiAmSar **1** with *N*-Boc-4-(bromomethyl)-benzylamine in the presence of sodium carbonate, which afforded the chelator **2** in 36% yield. After treatment with trifluoroacetic acid, intermediate **3** was conjugated to azido-PEG4-NHS ester, and monosubstituted product **4** was isolated in 61% yield. Finally, the chelator **4** was conjugated with a commercially available NIR fluorophore, sulfo-Cy5-NHS ester, in the presence of triethylamine. The fluorescently labeled starting material for the copper-catalyzed cycloaddition was isolated in 45% yield. All products were purified by HPLC and characterized by electrospray ionization mass spectrometry (ESI-MS).

In our current work, we used the GLP-1R targeting peptide exendin-4 ($E4_{x12}$), which was modified at the K_{12} position with the unnatural alkyne-amino acid (*S*)-2-amino-4-pentynoic acid (Figure 1A).[11,12,17] With the site-specific modification of the peptide with an alkyne and the attachment of an azide functional group to the chelator, we were able to perform a copper-catalyzed azide−alkyne cycloaddition (CuAAC) between $E4_{x12}$ and chelator **5**, using standard cycloaddition reaction conditions (buffered water, copper sulfate, ascorbic acid, room temperature) (Figure S1A). We obtained Cu-E4-Fl **6** in 20% yield over 1 h. HPLC and ESI-MS confirmed the identity of Cu-E4-Fl (Figure S1).

The radiolabeled bimodal imaging agent ^{64}Cu-E4-Fl **6** was synthesized using a one-pot synthetic protocol (Figure 1B). First, the fluorescently labeled sarcophagine **5** was complexed efficiently with ^{64}Cu in 0.5 M ammonium acetate buffer (radiochemical yield (RCY) ≥98%). The resulting ^{64}Cu-**5** was subjected to CuAAC reaction conditions using $E4_{x12}$, copper sulfate, and ascorbic acid, yielding the targeted bimodal imaging agent ^{64}Cu-E4-Fl **6**. ^{64}Cu loading was required before azide−alkyne conjugation to prevent saturation of the sarcophagine cage with cold copper. The synthetic preparation of ^{64}Cu-E4-Fl **6** can be achieved in 3 h (including radioisotope incorporation,

dx.doi.org/10.1021/bc500178d | *Bioconjugate Chem.* 2014, 25, 1323−1330

copper(I)-catalyzed [3 + 2] Huisgen cycloaddition, HPLC purification, evaporation of solvents, and formulation of an injectable solution) with an isolated decay-corrected RCY of 39%, a radiochemical purity ≥95%, and a specific activity of 141 μCi/μg. HPLC chromatograms of ^{64}Cu-E4-Fl **6** and its intermediates are shown in Figure 1C. Stability and competitive binding studies with ^{64}Cu-**5** were performed using an excess of $CuSO_4$, ascorbic acid, or EDTA. The high stability of ^{64}Cu-**5** was measured over 4 h, showing that the chelator has a suitable stability against trans-chelation (Figure 1D). Also, the sarcophagine cage shields ^{64}Cu(II) from reduction to ^{64}Cu(I) by ascorbic acid which could potentially lead to release of the PET radionuclide.

We evaluated the affinity of Cu-E4-Fl **6** to GLP-1R using an ^{125}I-exendin-4 (9−39) competitive binding assay (Figure 2A).[18]

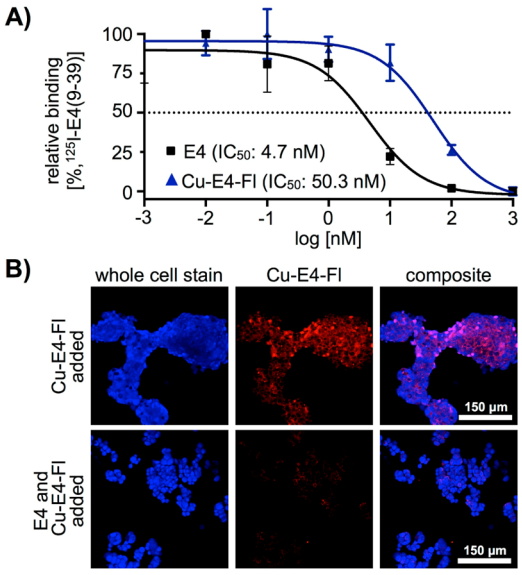

Figure 2. In vitro binding and inhibition studies. (A) IC_{50} value of Cu-E4-Fl **6**, measured via a competitive binding assay using HEK-hGLP1R cells. (B) Confocal microscopy imaging experiments using 916−1 insulinoma cells.

In comparison to exendin-4 with an IC_{50} of 4.7 ± 0.8 nM, we observed a slightly higher IC_{50} value of 50.3 ± 3.7 nM for our bimodal imaging tracer Cu-E4-Fl **6**. The binding affinity of Cu-E4-Fl **6** was confirmed in confocal cell imaging, where GLP-1R positive 916−1 insulinoma cells showed strong uptake (Figure 2B). After incubation with Cu-E4-Fl (10 nM or 100 nM, 90 min), cells were fixed and stained with Cellomics blue whole cell stain (Thermo Scientific, MA, USA), indicating internalization of the fluorescent imaging probe, similar to what was seen previously.[12] To show GLP-1R specificity of Cu-E4-Fl, we preincubated 916−1 cells with an excess of unmodified peptide $E4_{x12}$ (1 μM) before incubation with Cu-E4-Fl and observed suppressed fluorescent signal in the NIR (Figure 2B).

Similar to in vitro binding, ex vivo histology confirmed the selectivity of Cu-E4-Fl **6** to GLP-1R (Figure 3). One of the goals of developing GLP-1R targeting imaging agents is to use them as a β-cell targeting agent for delineating islets of Langerhans from exocrine pancreas. To show that ^{64}Cu-E4-Fl is selective for GLP-1R in vivo, we injected the imaging agent in MIP-GFP mice and let the agent circulate for 1 h, before nuclear cell stain was injected, the mice sacrificed, and pancreata harvested for histology. The GLP-1R targeted

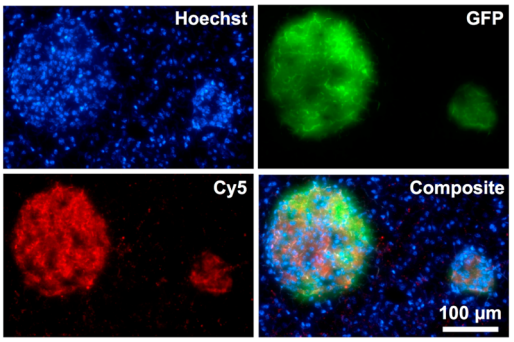

Figure 3. Fluorescence histology of a 10 μm pancreas section 1 h postinjection of Hoechst cell nuclear stain (top left) and ^{64}Cu-E4-Sar-Fl (bottom left) into transgenic mice with β-cell specific expression of GFP (top right). Green and red signal accumulations demonstrate islets of Langerhans. All images were acquired with an objective of 20×. Scale bar: 100 μm for all images.

^{64}Cu-E4-Fl probe showed a strong fluorescent signal in the 650 nm channel, colocalizing with the islets of Langerhans, as indicated by GFP fluorescence and similar to other GLP-1R imaging probes.[11,12]

In order to explore the potential applications of ^{64}Cu-E4-Fl **6** for in vivo imaging, we first determined the blood half-life of ^{64}Cu-E4-Fl (Figure 4A). After tail vein injection of the imaging

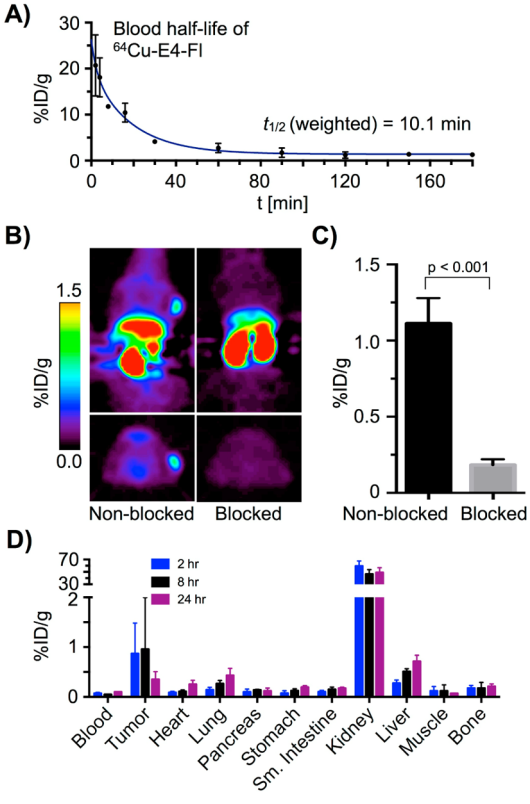

Figure 4. In vivo PET imaging with ^{64}Cu-E4-Fl. (A) Evaluation of the weighted blood half-life. (B) Decay-corrected small animal PET images (4−5 h) of 916−1 tumor-bearing (<2 mm) mice; intravenous injection of ^{64}Cu-E4-Fl (335 ± 35 μCi) in 200 μL PBS (4% DMSO) (nonblocked) and coinjection of ^{64}Cu-E4-Fl (335 ± 35 μCi) and $E4_{x12}$ (100 fold excess) in 200 μL PBS (4% DMSO). (C) Tumor uptake in nonblocked (1.1 ± 0.1%ID/g) and blocked (0.2 ± 0.1%ID/g) PET images. (D) Biodistribution study with 916−1 tumor bearing mice.

dx.doi.org/10.1021/bc500178d | Bioconjugate Chem. 2014, 25, 1323−1330

agent (30−35 μCi, n = 4), we observed a weighted $t_{1/2}$ of 10.1 min. The half-life was fitted to a two-phase exponential decay curve, resembling a multicompartment model with a fast agent distribution and a slow agent elimination phase.

With the purpose of determining the performance of ^{64}Cu-E4-Fl **6** as a whole body imaging agent, small animal PET imaging and ex vivo biodistribution studies were conducted using female nude mice bearing a subcutaneous insulinoma xenograft. In PET images, GLP-1R positive 916−1 tumors were easily visualized (Figure 4B). Other studies have shown before that exendin-4[12,19] and exendin-4 imaging agents[12] are rapidly internalized into cells, which allows imaging at later time points (5 h), when the probe had already cleared from the vasculature. To show specificity of ^{64}Cu-E4-Fl toward GLP-1R in whole body PET imaging, we further conducted blocking studies with unmodified peptide (100-fold excess). Small animal PET images confirmed effective blocking of 916−1 tumor uptake. Tumor ROI analysis of the PET data showed ^{64}Cu-E4-Fl **6** uptake of 1.1 ± 0.1%ID/g without and 0.2 ± 0.1%ID/g with preinjection of excess cold material (Figure 4C). Biodistribution data endorsed the observations derived from the PET data, as tumor uptake of 0.9 ± 0.6%ID/g and 1.0 ± 1.0%ID/g were observed after 2 and 8 h postinjection, respectively (Figure 4D).

We next compared the two different modalities of ^{64}Cu-E4-Fl at high resolution by using the radionuclide ^{64}Cu for phosphor autoradiography and the fluorochrome sulfo-Cy5 for fluorescent imaging (Figure 5A)—both on identical histology slides.

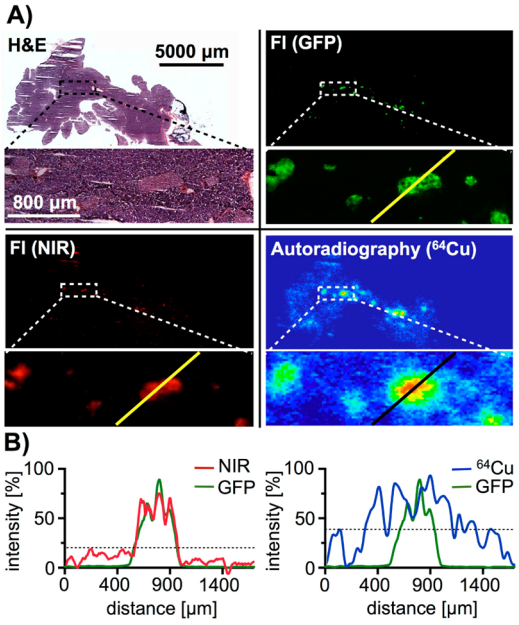

Figure 5. Comparison of autoradiographic and optical imaging for the visualization of β-cell mass. (A) H&E staining, fluorescent (GFP and NIR) and phosphor autoradiography images of a pancreatic histological slide (upper panels), as well as high magnification of an islet rich area (lower panels). (B) Signal intensity plots of a linear area of each imaging modality (GFP, NIR fluorescence, and autoradiography) image.

First, phosphor autoradiography was performed with a pancreatic section, followed by fluorescent imaging of the same histological slide to record the fluorescent signals of GFP and ^{64}Cu-E4-Fl. At both low and high resolution, there was a good correlation of both imaging modalities with regard to islet visualization. Intensity profile analysis, however, shows that the alignment of GFP positive areas and ^{64}Cu-E4-Fl is more accurate than the alignment of GFP positive areas and phosphor autoradiography. While the differences are less apparent at low resolution (Figure 5A), the comparison at high resolution (Figure 5B) illustrates the stark differences between fluorescence and autoradiography.

DISCUSSION

Over the past decades, PET has become standard of care as a clinical diagnostic tool, particularly in oncology. And while this technology has accelerated the understanding and detection of malignant growth,[20−23] it cannot provide the high spatial resolution typically associated with intravital imaging technologies.[4] The promise to merge the high spatial resolution of optical imaging probes with the sensitivity and whole body imaging capabilities of PET imaging motivated us in the design of multimodal imaging probes. In the past, different approaches and platforms were utilized for the synthesis of dual-modality PET/fluorescence imaging probes.[24−26] The challenge in designing bimodal imaging agents is that the sensitivity of different imaging modalities can vary by several orders of magnitude, and the half-life and biological stability of the imaging modalities should match each other. Also, modification of a targeted tracer with multiple imaging tags is more likely to lead to steric hindrance and can thus reduce the selectivity of an imaging probe. Compared to small molecules, peptides, and large biomolecules, the modular design and multifunctionality of nanoparticles enables the straightforward integration of different imaging modalities into one imaging agent and has made them the most commonly used platform for multimodal imaging agents.[27−30] However, the long circulation times of most nanoparticle-based imaging agents and their tendency to be taken up by macrophages can be a disadvantage for some clinical applications.

Based on the successful generation of bimodal sarcophagine-based imaging agents for peptides,[15,16,31] we aimed to develop a bioorthogonal bimodal imaging probe that can be conjugated site-selectively to a standard peptide. The bimodal NIR and ^{64}Cu bearing azide-modified linker **5** allows site-selective conjugation to a peptide without any protection/deprotection steps, and without any chemical modification of the peptide after solid phase synthesis and cleavage from the resin. This allows linker **5** to be used as a synthetic intermediate for one-step NIR/^{64}Cu labeling of a variety of peptides, and could allow the simultaneous labeling of multiple peptides with just one batch of ^{64}Cu-**5**. The radiolabeled ^{64}Cu-E4-Fl **6** is based on an alkyne-modified exendin-4 peptide, which was successfully used in the past for multiple exendin-4 imaging agents.[11,12,17,18] Recently, Clardy et al. showed that different positions of alkyne modifications in the peptide sequence lead to different binding affinities of the molecular imaging agent,[18] which could be one of the reasons for the lower binging affinity of ^{64}Cu-E4-Fl **6**, compared to the original peptide sequence.

To illustrate the advantages of a bimodal versus a monomodal imaging agent, we sectioned a MIP-GFP mouse pancreas after injection of ^{64}Cu-E4-Fl. Distributed within the pancreas of mice, rats, and humans are the islets of Langerhans, small cell clusters which amount for approximately 1−2% of the pancreatic mass and contain the targeted GLP-1R expressing β-cells.[32] Most islets are small and have diameters of only hundreds of micrometers, which makes them ideally suited to

dx.doi.org/10.1021/bc500178d | Bioconjugate Chem. 2014, 25, 1323−1330

compare autoradiography and fluorescence imaging. At low resolution (Figure 5A, upper panels), both autoradiography and fluorescence are mostly colocalized, indicating the bimodal imaging agent to be functional and intact. Imaging at higher magnification (Figure 5A, lower panels) and fluorescence intensity analysis (Figure 5B), however, show that NIR fluorescence intensity aligns better with the GFP islet signal than autoradiography. This, ultimately, illustrates the advantages of a bimodal imaging probe versus a monomodal PET or optical probe. After a single injection of ^{64}Cu-E4-Fl, we were able to show that both PET imaging as well as optical imaging is possible in the same animal, combining the advantages of whole body and high resolution imaging.

In conclusion, we have successfully developed an elegant, modular, and efficient method for the synthesis of a GLP-1R targeted peptidic bimodal PET/fluorescence imaging agent. We were able to conjugate a fluorescently labeled ^{64}Cu-chelated sarcophagine cage to an exendin-4 based targeted vector. We found that the copper-catalyzed [3 + 2] Huisgen cycloaddition does not result in quick trans-metalation between ^{nat}Cu and ^{64}Cu, resulting in good radiochemical purity and specific activities for the PET/fluorescence imaging probe. We demonstrated that ^{64}Cu-E4-Fl is capable of delineating GLP-1R expressing insulinoma with its whole body PET imaging tag and also pancreatic β-cell mass with its high resolution, low penetration optical imaging tag. We were able to show the advantages of optical imaging compared to autoradiography at high resolutions, allowing for more exact localization of imaging probes. We have shown that bimodal NIR/^{64}Cu labeling can be used to quickly design bimodal imaging probes, and that both functionalities can be utilized in one animal. Ultimately, we envision that probes like ^{64}Cu-E4-Fl could be used as hybrid imaging probes in the clinic, allowing the diagnosis of primary growths and metastases in a whole body imaging setting as well as real-time detection of tumor margins, infiltrative growth, or residual tumor cells in a surgical cavity.

EXPERIMENTAL PROCEDURES

Materials. Commercially available compounds were used without further purification unless otherwise stated. Acetonitrile (AcN) and dimethyl sulfoxide (DMSO) were purchased from Acros Organics as extra dry over molecular sieves. Alkyne-modified exendin-4 ($E4_{x12}$) was purchased from C S Bio Co. (Menlo Park, CA) and ^{125}I-exendin-4 (^{125}I-E4) was purchased from PerkinElmer (Boston, MA). Sarcophagine was obtained from Macrocyclics (Dallas, TX). Near-infrared (NIR) fluorophore sulfo-Cy5 *N*-hydroxysuccinimidyl (NHS) ester was purchased from Lumiprobe (Hallandale Beach, FL). Phosphate buffered saline (PBS) and Dulbecco's Modified Eagle Medium (DMEM) was purchased from the media preparation facility at Memorial Sloan Kettering Cancer Center (New York, NY, USA). All high performance liquid chromatography (HPLC) purifications (1.0 mL/min, Buffer A: 0.1% TFA in water, Buffer B: 0.1% TFA in AcN) were performed on a Shimadzu UFLC HPLC system equipped with a DGU-20A degasser, a SPD-M20A UV detector, a LC-20AB pump system, a CBM-20A communication BUS module, a FRC-10A fraction collector, and a Scan-RAM radio-TLC/HPLC-detector from LabLogic using a reversed phase Atlantis T3 column (C18, 5 μm, 4.6 mm × 250 mm). Electrospray ionization mass spectrometry (ESI-MS) spectra were recorded with a Waters Acquity UPLC (Milford, CA) with electrospray ionization SQ detector. High-resolution mass spectrometry (HRMS) spectra were recorded with a Waters LCT Premier system (ESI). Chelex-water was prepared with BT Chelex 100 Resin (Bio-Rad). Small animal PET imaging data were recorded on a microPET Focus 120. Digital phosphor autoradiography was achieved with a Typhoon FLA 7000 laser scanner from GE Healthcare. The radioactivity of organs for biodistribution studies was counted with a WIZARD^2 automatic γ-counter from PerkinElmer and the radioactivity of the binding assay was counted with a Wallac 3″ 1480 Automatic γ-counter. Histology slides of 10 μm fresh-frozen sliced sections of pancreas were analyzed with an Olympus BX-60 microscope equipped with a CoolSNAP EZ camera from Photometrics for fluorescent pictures, a CC12 Soft Imaging Systems camera from Olympus for RGB pictures, a Olympus UPlanFl objective with a 10× magnification, and a Olympus UPlanApo objective with a 20× magnification. MicroSuite FIVE software was used to register images, and Adobe Photoshop and Fiji software was used to manually adjust and analyze images.

Preparation of Di-BnAm(Boc)-Sar 2. *N*-Boc-4-(bromomethyl)-benzylamine (0.019 g, 0.064 mmol, 1.3 equiv) was added slowly to a stirred solution of DiAmSar **1** (0.015 g, 0.049 mmol, 1.0 equiv) in dry dimethylformamide (3.0 mL) under nitrogen at room temperature. After addition of sodium carbonate (0.018 g, 0.16 mmol, 2.6 equiv) the reaction solution was stirred at 70 °C for 16 h. The reaction mixture was allowed to warm to room temperature and diluted with water (9.0 mL). Purification by HPLC (1 mL/min, 5% to 80% B in 15 min) afforded **2** (0.014 g, 36%) as a colorless solid: t_R = 11.2 min. ESI-MS(+): m/z (%) = 753.55 (100) $[M + H]^+$. HRMS (ESI): m/z calcd for $C_{40}H_{69}N_{10}O_4$: 753.5498; found: 753.5502.

Preparation of Di-BnAm-Sar 3. Trifluoroacetic acid (2.0 mL) was added slowly to a stirred solution of **2** (7.1 mg, 9.4 μmol, 1.0 equiv) in dry acetonitrile (2.0 mL) and the reaction mixture was stirred at room temperature for 1 h. Evaporation of the solvents under reduced pressure and purification by HPLC (1 mL/min, 5% to 80% B in 15 min) afforded **3** (4.5 mg, 86%) as a colorless oil: t_R = 7.2 min. ESI-MS(+): m/z (%) = 277.25 (100) $[M+2H]^+$, 553.48 (50) $[M + H]^+$. HRMS (ESI): m/z calcd for $C_{30}H_{52}N_{10}$: 553.4455; found: 553.4467.

Preparation of azido-PEG4-Di-BnAm-Sar 4. A solution of azido-PEG4-NHS ester (1.4 mg, 7.2 μmol, 1.0 equiv) in dimethylformamide (140 μL) was added slowly to a 0 °C cooled solution of **3** (4.0 mg, 7.2 μmol, 2.0 equiv) in dimethylformamide (500 μL). After addition of triethylamine (1.0 μL, 0.73 mg, 7.2 μmol, 2.0 equiv) the reaction mixture was stirred gently at room temperature for 2 h. Dilution with water (2.0 mL) and purification by HPLC (1.0 mL/min, 5% to 80% B in 15 min) afforded **4** (1.8 mg, 61%) as a colorless oil: t_R = 8.8 min. ESI-MS(+): m/z (%) = 414.08 (100) $[M+2H]^{2+}$, 827.00 (10) $[M + H]^+$.

Preparation of sulfo-Cy5-azido-PEG4-Di-BnAm-Sar 5. A solution of sulfo-Cy5-NHS ester (1.0 mg, 1.3 μmol, 1.1 equiv) in dry dimethylformamide (200 μL) was added slowly to a 0 °C cooled solution of **4** (1.0 mg, 1.2 μmol 1.0 equiv) in dry dimethylformamide (500 μL). After addition of triethylamine (0.4 μL, 0.3 mg, 2.6 μmol, 2.2 equiv) the reaction mixture was stirred gently at room temperature for 2 h. Dilution with water (2.0 mL) and purification by HPLC (5% to 40% B in 15 min) afforded **5** (0.8 mg, 45%) as a blue solid: t_R = 15.7 min. ESI-MS(−): m/z (%) = 1449.60 (5) $[M-Na]^-$. ESI-MS(+): m/z (%) = 370.34 (100) $[M+4H]^{4+}$, 747.92 (40) $[M+Na+H]^{2+}$, 1452.12 (15) $[M-Na+2H]^+$.

dx.doi.org/10.1021/bc500178d | *Bioconjugate Chem.* 2014, 25, 1323−1330

Preparation of Cu-E4-Fl 6. To a solution of azide **5** (0.60 mg, 0.41 μmol, 1.0 equiv) and alkyne-modified exendin-4 ($E4_{x12}$) (1.6 mg, 0.41 μmol, 1.0 equiv) in PBS (300 μL) was added a premixed solution of $CuSO_4$ (10 mM in PBS, 1.6 mg) and L-ascorbic acid (50 mM in PBS, 4.4 mg) in PBS (2.0 mL) to the reaction mixture and stirred gently at room temperature in the dark for 1 h. Purification by HPLC (1.0 mL/min, 0% to 60% B in 18 min) afforded Cu-E4-Fl **6** (0.46 mg, 20%) as a blue solid: t_R = 16.4 min. ESI-MS(+): *m*/*z* (%) 1134.41 (100) $[M+5H]^{5+}$, 1417.95 (35) $[M+4H]^{4+}$.

Preparation of ^{64}Cu-E4-Fl 6. $^{64}CuCl_2$ (3.5 μL, 1.98 mCi, 73.3 MBq) was added to a solution of synthesized azide **5** (174 mM in chelex-water, 19.2 μL, 5 μg) in ammonium acetate buffer (0.5 M in H_2O, 100 μL, pH 5.4) and the reaction mixture was kept at 37 °C for 45 min. Analytical HPLC (0.8 mL/min, 0% to 90% B in 17 min) revealed formation of ^{64}Cu-**5** (t_R = 15.2 min) in ≥98% radiochemical yield (specific activity 396 μCi/μg). A solution of $E4_{x12}$ (240 μM in PBS, 20 μL, 20 μg) was added to the radiolabeled precursor. A solution of $CuSO_4$ (10 mM in PBS, 0.8 mg) in PBS (500 μL) was added to a solution of L-ascorbic acid (50 mM in PBS, 4.4 mg) in PBS (500 μL) and the solution was stirred for 5 min at room temperature. Afterward a premixed $CuSO_4$/L-ascorbic acid solution (100 μL) was added to the reaction mixture and stirred at room temperature in the dark for 1 h. The crude mixture was subjected to HPLC purification (0.8 mL/min, 0% to 90% B in 17 min) affording ^{64}Cu-E4-Fl **6** (706 μCi, isolated decay-corrected radiochemical yield: 39%, specific activity: 141 μCi/μg, radiochemical purity: ≥95%). The solvents were evaporated to dryness and ^{64}Cu-E4-Fl **6** was reconstituted in a solution of PBS (400 μL) and DMSO (20 μL).

Competition Study of ^{64}Cu-5 with $CuCl_2$. A solution of $CuCl_2$ (80 μL, 40 mM in PBS, 2.1 mg) was added to a solution of ^{64}Cu-**5** (35 μL, 290−310 μCi). At predetermined time points (0.0, 0.5, 1.5, and 4 h) a sample of the competition solution (10 μL) was added to an EDTA-solution (50 mM in Chelex-water, 40 μL) and subjected to analytical HPLC purification (0.8 mL/min, 0% to 90% B in 17 min). The competition study was performed in triplicate.

Stability Study of ^{64}Cu-5 with Ascorbic Acid. A solution of ascorbic acid (150 μL, 150 mM in PBS, 13 mg) was added to a solution of ^{64}Cu-**5** (30 μL, 290−310 μCi). At predetermined time points (0.0, 0.5, 1.5, and 4 h) a sample of the competition solution (10 μL) was added to an EDTA-solution (50 mM in Chelex-water, 40 μL) and subjected to analytical HPLC purification (0.8 mL/min, 0% to 90% B in 17 min). The stability study was performed in triplicate.

Cell Culture. The human embryonic kidney cells HEK-hGLP1R, a GLP-1R positive cell line, were used for the receptor binding study. Cell culture was performed as previously described.[18] The cells were grown in high-glucose DMEM containing 10% (v/v) heat-inactivated FBS, 50 U/mL penicillin, 10 μg/mL streptomycin, 1 mM sodium pyruvate, and 150 μg/mL G418 (Geneticin). 916−1, a GLP-1R positive insulinoma cell line was a gift from Dr. Johanna Joyce (Memorial Sloan Kettering Cancer Center, New York, USA). The cells were grown in Dulbecco's Modified Eagle Medium (DMEM) supplemented with heat-inactivated fetal bovine serum (10% v/v), penicillin (100 units/mL), and streptomycin (100 μg/mL) and passaged regularly at 50−60% confluence in a ratio of 1:2eVery 3−4 days. The cells were used for in vitro binding assays and in vivo xenograft mouse models at passages 18−20. 916−1 and HEK-hGLP1R cells were cultured according to the recommendations of American Type Culture Collection and Caliper Life Sciences under 37 °C with 5% CO_2.

In Vitro Receptor Binding Assay. A previously described receptor binding assay[18] was used to determine the receptor binding affinity of Cu-E4-Fl **6**. HEK-hGLPR1R cells were seeded in a 96 well plate (5.5×10^4 cells per well) and grown at 37 °C for 48 h. After washing with binding buffer (120 mM NaCl, 1.2 mM $MgSO_4$, 13 mM sodium acetate, 5 mM KCl, 1.2 g/L Tris, 2 g/L bovine selum albumin (BSA), and 1.8 g/L glucose, pH 7.6) the cells were cotreated with 30 pM of ^{125}I-exendin-4 (9−39, PerkinElmer, Boston, MA) and Cu-E4-Fl (final concentration range: 10^{-12}−10^{-6} M). After incubation at 37 °C for 2 h, cells were washed with PBS (3 × 150 μL) containing 1 mg/mL BSA, lysed (RIPA 1× buffer, 15 min) and the radioactivity of contents were measured using a Wallac 3″ 1480 Automatic γ-counter.

In Vitro Cell Imaging. To determine in vitro probe uptake, 916−1 cells (2.5×10^5 per well) were seeded in an 8-well chamber slide (Lab-TekII Chamber Slide) and incubated at 37 °C for 48 h. Afterward the cells were incubated with just Cu-E4-Fl (10 nM or 100 nM in PBS containing 3% DMSO, 37 °C for 90 min) or underwent a preincubation with $E4_{x12}$ (1 μM in PBS, 37 °C for 30 min, 1× wash with 250 μL medium) before incubation with Cu-E4-Fl (10 nM or 100 nM in PBS containing 3% DMSO, at 37 °C for 90 min) in fresh media (250 μL). After washing with growth media (150 μL) and PBS (2 × 150 μL), blue whole cell stain (Thermo Scientific Cellomics Whole CellStain) was added and incubated at room temperature for 20 min. The cells were washed with PBS (2 × 150 μL), fixed with 4% paraformaldehyde (150 μL), and agitated at room temperature for 5 min. The wells were washed with PBS (150 μL) before removing chambers and adding mounting media and coverslip. The cells were imaged using a confocal microscope (Leica TCS SP5 II).

Animals. All animal experiments and procedures were carried out in accordance with the guidelines set by the Institutional Animal Care and Use Committee at Memorial Sloan Kettering Cancer Center. Transgenic homozygous B6.Cg-Tg(Ins1-GFP)1Hara/J mice, which express GFP under the control of mouse insulin 1 promoter (MIP-GFP), were obtained from the Jackson laboratory and bred at 6−8 weeks of age. The resulting litters were used for pancreatic β-cell mass imaging. Female athymic nude mice (Taconic Lab; CrTac:NCr-Foxn1nu, 6−8 weeks, 20−22 g) were induced with tumors on the right shoulder. 916−1 insulinoma cells (3.0×10^6) were suspended in a 1:1 mixture of media and matrigel (150 μL) and injected subcutaneously to establish xenograft tumor mouse models (<2 mm tumor volume) after 3 weeks.

Blood Half-Life. Female nude mice (6−8 weeks, *n* = 4) were injected with ^{64}Cu-E4-Fl (30−35 μCi) in PBS (5% DMSO, 200 μL) via lateral tail vein. At predetermined time points (2, 4, 8, 16, 30, 60, 90, 120, 150, and 180 min), a blood sample was obtained from the great saphenous vein of each animal. The radioactivity of the blood samples was recorded with a WIZARD^2 automatic γ-counter from PerkinElmer and the weights of collected blood samples were determined. The percentage of tracer uptake expressed as a percentage injected dose per gram (%ID/g) was calculated as the activity present in the blood weight per actual injected dose, decay-corrected to the time of counting.

Biodistribution. 916−1 tumor-bearing nude mice were used for evaluating the biodistribution of ^{64}Cu-E4-Fl in the whole body. Mice (6−8 weeks, *n* = 12) were injected with

^{64}Cu-E4-Fl (30−40 μCi) in PBS (5% DMSO, 200 μL) via tail vein injection. At predetermined time points (2, 6, and 24 h after injection) the mice were sacrificed by asphyxiation with CO_2 and blood was collected via cardiac puncture. Selected organs (tumor, heart, lung, spleen, pancreas, stomach, small intestine, large intestine, kidney, liver, muscle, bone, and tail) were harvested, weighed, and counted using a WIZARD^2 automatic γ-counter from PerkinElmer. The percentage of tracer uptake stated as percentage injected dose per gram of tissue (%ID/g) was calculated as the activity bound to tissue per organ weight per actual injected dose, decay-corrected to the start time of counting.

PET Imaging. Small animal PET imaging data were recorded on a microPET Focus 120. ^{64}Cu-E4-Fl (335 ± 35 μCi) in PBS (4% DMSO, 200 μL) was injected into the tumor-bearing nude mice (n = 7) via tail vein. At 5−6 h after the injection, the mice were anesthetized with 1.5−2.0% isoflurane (Baxter Healthcare) at 2 L/min in oxygen and PET images were recorded over 10 min. An additional group of nude mice (n = 5) was injected with ^{64}Cu-E4-Fl (335 ± 35 μCi) premixed with unlabeled exendin-4 (100-fold excess) in PBS (4% DMSO, 200 μL) as a blocking agent and to determine the specificity of E4 to GLP-1 receptors. Images were analyzed using AsiPro VM software (Concorde Microsystems). Quantification of activity concentration in the xenograft tumor was done by drawing region of interests (ROIs) in four different slices and averaging the maximum values.

Digital Phosphor Autoradiography of Histological Pancreatic Slides. For digital autoradiography experiments, ^{64}Cu-E4-Fl (335 ± 35 μCi) in PBS (4% DMSO, 200 μL) was injected into transgenic B6.Cg-Tg(Ins1-EGFP)1Hara/J mice (n = 5) via tail vein. Hoechst 33342 nuclear cell stain (150 μL, 10 mg/mL) was injected 1 h after tracer injection and the mouse was sacrificed after an additional 5 min. The harvested pancreata were flash-frozen (dry ice) in Tissue-Tek O.C.T. compound (Sakura Finetek, Torrance, CA), cut into 10 μm sections, and exposed to a phosphor-imaging plate (Fujifilm BAS-MS2325, Fuji Photo Film, Japan) for 24 h at −20 °C. After completion of exposure, the imaging plates were analyzed using a Typhoon FLA 7000 laser scanner (GE Healthcare, Port Washington, NY) with 25 μm pixel resolution.

Fluorescence Microscopy of Histological Pancreatic Slides. The same slides were used both for digital autoradiography and fluorescence microscopy. Histology images of 10 μm fresh-frozen sliced sections were analyzed using an Olympus BX-60 microscope equipped with a CoolSNAP EZ camera (Photometrics, Tucson, AZ) for fluorescent pictures, a CC12 Soft Imaging Systems camera (Olympus, Hauppauge, NY) for RGB pictures, a Olympus UPlanFl objective with 10× magnification, and a Olympus UPlanApo objective with 20× magnification. Fluorescence images were obtained using appropriate filter cubes for each wavelength (Hoechst, GFP, and NIR fluorescence). A computer controlled motorized stage allowed images of whole sections to be generated as a mosaic with a 10× magnification with identical exposure time per frame. MicroSuite FIVE software was used to fuse images and Adobe Photoshop and Fiji software was used to manually adjust and analyze images.

■ ASSOCIATED CONTENT

Ⓢ Supporting Information

Additional schemes and figures. This material is available free of charge via the Internet at http://pubs.acs.org/.

■ AUTHOR INFORMATION

Corresponding Author

*E-mail: reinert@mskcc.org; Phone: +1 646 888 3461.

Notes

The authors declare no competing financial interest.

■ ACKNOWLEDGMENTS

The authors thank the Small Animal Imaging Core as well as the Radiochemistry and Molecular Imaging Probes Core (P30 CA008748-48, S10 RR020892-01) for support. The authors thank Valerie Longo, Carlos Perez-Medina, and Naga Vara Kishore Pillarsetty for helpful discussions. The authors also thank Johanna Joyce (MSKCC) for cell lines. Finally, the study was supported by grants from the National Institute of Health (K25 EB016673 for T.R.), the Brain Tumor Center of Memorial Sloan Kettering Cancer Center, as well as the Center for Molecular Imaging and Nanotechnology of Memorial Sloan Kettering Cancer Center (for T.R.).

■ REFERENCES

(1) Margolis, D. J. A., Hoffman, J. M., Herfkens, R. J., Jeffrey, R. B., Quon, A., and Gambhir, S. S. (2007) Molecular imaging techniques in body imaging. *Radiology 245*, 333−356.

(2) Louie, A. (2010) Multimodality imaging probes: design and challenges. *Chem. Rev. 110*, 3146−3195.

(3) Rudin, M., and Weissleder, R. (2003) Molecular imaging in drug discovery and development. *Nat. Rev. Drug Discovery 2*, 123−131.

(4) Pittet, M. J., and Weissleder, R. (2011) Intravital imaging. *Cell 147*, 983−991.

(5) Zanzonico, P. (2012) Principles of nuclear medicine imaging: planar, SPECT, PET, multi-modality, and autoradiography systems. *Radiat. Res. 177*, 349−364.

(6) Thurber, G. M., Figueiredo, J., and Weissleder, R. (2010) Detection limits of intraoperative near infrared imaging for tumor resection. *J. Surg. Oncol. 102*, 758−764.

(7) Jennings, J. E., and Long, N. J. (2009) 'Two is better than one'-probes for dual-modality molecular imaging. *Chem. Commun. 49*, 3511−3524.

(8) Li, C., Wang, W., Wu, Q., Ke, S., Houston, J., Sevick-Muraca, E., Dong, L., Chow, D., Charnsangavej, C., and Gelovani, J. G. (2006) Dual optical and nuclear imaging in human melanoma xenografts using a single targeted imaging probe. *Nucl. Med. Biol. 33*, 349−358.

(9) Christ, E., Wild, D., Ederer, S., Béhé, M., Nicolas, G., Caplin, M. E., Brändle, M., Clerici, T., Fischli, S., and Stettler, C. (2013) Glucagon-like peptide-1 receptor imaging for the localisation of insulinomas: a prospective multicentre imaging study. *Lancet Diabetes Endocrinol. 1*, 115−122.

(10) Wild, D., Christ, E., Caplin, M. E., Kurzawinski, T. R., Forrer, F., Brandle, M., Seufert, J., Weber, W. A., Bomanji, J., Perren, A., Ell, P. J., and Reubi, J. C. (2011) Glucagon-like peptide-1 versus somatostatin receptor targeting reveals 2 distinct forms of malignant insulinomas. *J. Nucl. Med. 52*, 1073−1078.

(11) Reiner, T., Kohler, R. H., Liew, C. W., Hill, J. A., Gaglia, J., Kulkarni, R. N., and Weissleder, R. (2010) Near-infrared fluorescent probe for imaging of pancreatic beta cells. *Bioconjugate Chem. 21*, 1362−1368.

(12) Reiner, T., Thurber, G., Gaglia, J., Vinegoni, C., Liew, C. W., Upadhyay, R., Kohler, R. H., Li, L., Kulkarni, R. N., Benoist, C., Mathis, D., and Weissleder, R. (2011) Accurate measurement of pancreatic islet beta-cell mass using a second-generation fluorescent exendin-4 analog. *Proc. Natl. Acad. Sci. U. S. A. 108*, 12815−12820.

(13) Wild, D., Behe, M., Wicki, A., Storch, D., Waser, B., Gotthardt, M., Keil, B., Christofori, G., Reubi, J. C., and Maecke, H. R. (2006) [Lys^{40}(Ahx-DTPA-^{111}In)NH_2)exendin-4, a very promising ligand for glucagon-like peptide-1 (GLP-1R) receptor targeting. *J. Nucl. Med. 47*, 2025−2033.

(14) Wild, D., Wicki, A., Mansi, R., Behe, M., Keil, B., Bernhardt, P., Christofori, G., Ell, P. J., and Macke, H. R. (2010) Exendin-4-based radiopharmaceuticals for glucagonlike peptide-1 receptor PET/CT and SPECT/CT. *J. Nucl. Med. 51*, 1059−1067.
(15) Liu, S., Li, D., Huang, C. W., Yap, L. P., Park, R., Shan, H., Li, Z., and Conti, P. S. (2012) The efficient synthesis and biological evaluation of novel bi-functionalized sarcophagine for ^{64}Cu radiopharmaceuticals. *Theranostics 2*, 589−596.
(16) Liu, S., Li, D., Huang, C. W., Yap, L. P., Park, R., Shan, H., Li, Z., and Conti, P. S. (2012) Efficient construction of PET/fluorescence probe based on sarcophagine cage: an opportunity to integrate diagnosis with treatment. *Mol. Imaging Biol. 14*, 718−724.
(17) Keliher, E. J., Reiner, T., Thurber, G. M., Upadhyay, R., and Weissleder, R. (2012) Efficient ^{18}F-labeling of synthetic exendin-4 analogues for imaging beta cells. *ChemistryOpen 1*, 177−183.
(18) Clardy, S. M., Keliher, E. J., Mohan, J. F., Sebas, M., Benoist, C., Mathis, D., and Weissleder, R. (2013) Fluorescent exendin-4 derivatives for pancreatic beta-cell analysis. *Bioconjugate Chem. 25*, 171−177.
(19) Widmann, C., Dolci, W., and Thorens, B. (1995) Agonist-induced internalization and recycling of the glucagon-like peptide-1 receptor in transfected fibroblasts and in insulinomas. *Biochem. J. 310*, 203−214.
(20) Adams, S., Baum, R. P., Stuckensen, T., Bitter, K., and Hör, G. (1998) Prospective comparison of ^{18}F-FDG PET with conventional imaging modalities (CT, MRI, US) in lymph node staging of head and neck cancer. *Eur. J. Nucl. Med. 25*, 1255−1260.
(21) Delbeke, D. (1999) Oncological applications of FDG PET imaging: brain tumors, colorectal cancer, lymphoma and melanoma. *J. Nucl. Med. 40*, 591−603.
(22) Duhaylongsod, F. G., Lowe, V. J., Patz, E. F., Jr, Vaughn, A. L., Coleman, R. E., and Wolfe, W. G. (1995) Lung tumor growth correlates with glucose metabolism measured by fluoride-18 fluorodeoxyglucose positron emission tomography. *Ann. Thorac. Surg. 60*, 1348−1352.
(23) Schiepers, C., Penninckx, F., De Vadder, N., Merckx, E., Mortelmans, L., Bormans, G., Marchal, G., Filez, L., and Aerts, R. (1995) Contribution of PET in the diagnosis of recurrent colorectal cancer: comparison with conventional imaging. *Eur. J. Surg. Oncol. 21*, 517−522.
(24) Pandey, S. K., Gryshuk, A. L., Sajjad, M., Zheng, X., Chen, Y., Abouzeid, M. M., Morgan, J., Charamisinau, I., Nabi, H. A., Oseroff, A., and Pandey, R. K. (2005) Multimodality agents for tumor imaging (PET, fluorescence) and photodynamic therapy. A possible "see and treat" approach. *J. Med. Chem. 48*, 6286−6295.
(25) Ranyuk, E., Lebel, R., Berube-Lauziere, Y., Klarskov, K., Lecomte, R., van Lier, J. E., and Guerin, B. (2013) ^{68}Ga/DOTA- and ^{64}Cu/NOTA-phthalocyanine conjugates as fluorescent/PET bimodal imaging probes. *Bioconjugate Chem. 24*, 1624−1633.
(26) Liu, S., Conti, P. S., and Li, Z. (2013) PET/Fluorescence imaging: an opportunity to integrate diagnosis with surgery. *J. Radiology 2*, e115.
(27) Kim, J., Piao, Y., and Hyeon, T. (2009) Multifunctional nanostructured materials for multimodal imaging, and simultaneous imaging and therapy. *Chem. Soc. Rev. 38*, 372−390.
(28) Kircher, M. F., Mahmood, U., King, R. S., Weissleder, R., and Josephson, L. (2003) A multimodal nanoparticle for preoperative magnetic resonance imaging and intraoperative optical brain tumor delineation. *Cancer Res. 63*, 8122−8125.
(29) Veiseh, O., Sun, C., Gunn, J., Kohler, N., Gabikian, P., Lee, D., Bhattarai, N., Ellenbogen, R., Sze, R., Hallahan, A., Olson, J., and Zhang, M. (2005) Optical and MRI multifunctional nanoprobe for targeting gliomas. *Nano Lett. 5*, 1003−1008.
(30) Weissleder, R., Kelly, K., Sun, E. Y., Shtatland, T., and Josephson, L. (2005) Cell-specific targeting of nanoparticles by multivalent attachment of small molecules. *Nat. Biotechnol. 23*, 1418−1423.
(31) Liu, S., Li, Z., Yap, L. P., Huang, C. W., Park, R., and Conti, P. S. (2011) Efficient preparation and biological evaluation of a novel multivalency bifunctional chelator for ^{64}Cu radiopharmaceuticals. *Chemistry 17*, 10222−10225.
(32) Elayat, A. A., el-Naggar, M. M., and Tahir, M. (1995) An immunocytochemical and morphometric study of the rat pancreatic islets. *J. Anat. 186*, 629−637.